

# Effect of Solution Treatment on Grain Growth and Precipitates in Electroslag Remelted 15Cr-22Ni Iron-Base Superalloy



XIN ZHENG, CHENGBIN SHI, XIN ZHU, JING LI, and HAOCHI XU

The effects of solution temperature and soaking time on the grain growth and precipitates in a novel iron-base superalloy were investigated. Abnormal grain growth occurs at the solution temperature of 1473 K (1200 °C) irrespective of the niobium content and soaking time, which is attributed to the dissolution and coarsening of NbC precipitates. The amount of NbC particles increases with increasing niobium content of the superalloy, which has a strong pinning effect on grain boundary migration. Fe<sub>2</sub>Nb-type Laves phase is fully dissolved in the superalloy containing 0.64 and 1.00 mass pct Nb, whereas eutectic carbide NbCs are partially dissolved regardless of the solution temperatures. Both Fe<sub>2</sub>Nb-type Laves phase and eutectic carbide NbC are partially dissolved in the superalloy with 1.40 mass pct Nb after the solution at 1443 K (1170 °C) because of the competitive dissolution of Fe<sub>2</sub>Nb-type Laves phase and eutectic carbide NbC. The amount of eutectic carbides NbC after the solution at 1473 K (1200 °C) is larger than that at 1443 K (1170 °C) because of higher soluble niobium content in the superalloy matrix contributed by the complete dissolution of Fe<sub>2</sub>Nb-type Laves phase. A model for predicting the austenite grain growth of the superalloy with varying niobium contents during solution is developed. The role of niobium on the hardness of the superalloy was discussed.

<https://doi.org/10.1007/s11663-021-02421-1>

© The Minerals, Metals & Materials Society and ASM International 2022, corrected publication 2022

## I. INTRODUCTION

15Cr-22Ni iron-base superalloy is widely used in the gas turbine industry and aero-engines because of its good high-temperature properties (*i.e.*, creep strength, tensile strength and stability performance) and cost-effective nature,<sup>[1–3]</sup> such as turbine bucket, wheel and fastener products serving at moderately elevated temperatures. 15Cr-22Ni iron-base superalloy is in the family of precipitation-hardening austenitic heat-resistant steel. The strengthening by fine dispersed precipitates is a crucial strengthening strategy for Ni-Cr-type iron-base superalloy,<sup>[4]</sup> such as A286 and SUH660. The size, distribution and thermal stability of precipitates have a significant effect on the high-temperature properties of metallic materials.<sup>[5,6]</sup>

Niobium is a strong Laves phase-forming element. Laves phase is a AB<sub>2</sub>-type intermetallic compound with a hexagonal C14 structure. Previous studies<sup>[7–10]</sup> indicate that Fe<sub>2</sub>Nb-type Laves phase is an effective and stable phase which has been widely employed to improve the tensile strength and creep strength of alloy and steel. Meanwhile, the steel and superalloy are alloyed with niobium with an aim to form fine and well-dispersed NbC precipitates for pinning austenite grain boundaries at high temperatures and ultimately for restraining austenite grain growth.<sup>[11]</sup> Niobium can also act as solute atom to produce solute drag effect on austenite grain boundaries and inhibit the austenite grain growth.<sup>[12]</sup> The pinning effect and solute drag effect would retard the decrease in both tensile strength and plasticity of the superalloy caused by austenite grain coarsening.<sup>[13]</sup> Large carbides and intermetallic compounds are inevitably precipitated in iron-base superalloy because of high concentrations of alloying elements in the superalloy.<sup>[8,14]</sup> These large precipitates are detrimental to the workability and plasticity of the superalloy.<sup>[15,16]</sup>

Solution treatment is an essential processing process for manufacturing some varieties of superalloys and steels aiming to not only maximumly dissolve large precipitates, but also achieve uniform distribution of the alloying elements that dissociated from large precipitates in the matrix.<sup>[17]</sup> However, unsuitable holding

---

XIN ZHENG, CHENGBIN SHI, XIN ZHU, JING LI, and HAOCHI XU are with the State Key Laboratory of Advanced Metallurgy, University of Science and Technology Beijing (USTB), Beijing, 100083, P.R. China. Contact e-mail: chengbin.shi@ustb.edu.cn  
Manuscript submitted September 29, 2021; accepted December 19, 2021.

temperature and soaking time of solution treatment would result in severe coarsening of austenite grains.<sup>[18]</sup> Shirdel *et al.*<sup>[19]</sup> revealed the transition of grain growth mode from normal to abnormal during solution of austenite stainless steel at 1173K (900 °C) and the subsequent reappearance of normal growth mode with increasing the soaking time to 720 minutes. Chamanfar *et al.*<sup>[20]</sup> reported that the solution temperature plays a dominant role in the transition of austenite grain growth from abnormal to normal. Xu *et al.*<sup>[18]</sup> demonstrated that the solution temperature was the dominant factor affecting austenite grain growth of 12Cr rotor steel, and the amount of carbides and nitrides was considerably reduced at the solution temperatures of 1050 °C and 1150 °C. Their full dissolution was achieved at 1250 °C. Failure typically occurs at the grain boundaries during high-temperature service of superalloy and steel. Coarsened grains would reduce the number of grain boundaries and free energy of the grain boundary.<sup>[17]</sup> The severe coarsening of austenite grains generally leads to a decrease in the both plasticity and toughness of steel and alloy.<sup>[21,22]</sup> Besides the pinning force contributed by carbides and nitrides, fine Laves phase can also serve an effective role in pinning austenite grains.<sup>[8,16]</sup> Previous studies<sup>[8,13,16-21]</sup> have confirmed that the austenite grain growth during solution treatment is closely related to the compositions of alloy, and the size, types and distribution of the precipitates, besides the solution processing parameters.

Complicated evolution of microstructure generally occurs during the high-temperature solution processing of metallic materials, including recrystallization, grain growth, pinning effect and grain boundary characteristics. For the newly designed 15Cr-22Ni iron-base superalloy strengthened by carbides and Laves phase, it is necessary to develop solution processing parameters for maximizing dissolution of large carbides and Laves phase, together with obtaining reasonable austenite grain size simultaneously. In the current study, the grain growth of 15Cr-22Ni iron-base superalloy with varying niobium contents at different solution temperatures and soaking time was investigated. The precipitates in the superalloy with different niobium contents before and after solution were characterized. Moreover, a grain growth model was established. The effect of niobium on the size and amount of carbides and Laves phase as well as austenite grains in the newly developed iron-base superalloy under different solution conditions was ascertained. The mechanism of hardness variation of the superalloy was analyzed.

## II. EXPERIMENTAL

### A. Materials and Solution Treatment

15Cr-22Ni iron-base superalloy with three different niobium contents (0.64, 1.00 and 1.40 mass pct) was prepared using vacuum induction melting, followed by electroslag remelting to produce as-cast ingot with a diameter of 180 mm. The chemical compositions of the

superalloy ingots are shown in Table I. These as-cast ingots were forged into billets with 70 mm × 70 mm in cross-section after being held at 1433 K (1160 °C) for 3 hours, followed by air cooling to ambient temperature. The forging finish temperature was no lower than 1223 K (950 °C). The specimens that were taken from the forged alloy were solution treated at 1443 K, 1473 K and 1503 K (1170 °C, 1200 °C and 1230 °C) for 0.5 to 4 hours and then immediately quenched in water.

### B. Microstructure Characterization and Vickers Hardness Measurement

The specimens that were taken from solution-treated superalloy were ground with abrasive papers, followed by being polished with diamond paste. The cross-sections of metallographic specimens were etched with a solution of 50 mL sulfuric acid and 1 g potassium permanganate at 358 K (85 °C) for 10 minutes and then examined by optical microscope (DM4 M, Leica) to observe the microstructure. The optical microscopy (OM) images were randomly selected for determining the grain size of the solution-treated superalloys. The grain sizes of these specimens were determined by line-intercept method. The image analysis was performed using Image-Pro Plus 6.0 software.

The etched cross-sections of metallographic specimens were analyzed by scanning electron microscope (SEM, FEI Quanta-250; FEI Corporation, Hillsboro, OR) equipped with an energy-dispersive x-ray spectrometer (EDS, XFlash 5030; Bruker, Germany) and field emission scanning electron microscope (FE-SEM, Regulus8100, Hitachi, Japan) equipped with energy dispersive x-ray spectroscopy (EDS, XFlash 5030; Bruker, Germany) to observe the precipitates. The specimens for the electron backscatter diffraction (EBSD, Oxford Symmetry, UK) analysis were electropolished in 10 pct perchloric acid and 90 pct ethanol solution.

Vickers hardness tests were performed on a hardness tester (THV-1MDX, China) with a load of 100 g and a dwell time of 15 seconds. The value of Vickers hardness presented in this article is an average of five measurements.

## III. RESULTS AND DISCUSSION

### A. Growth Behavior of Austenite Grain

#### 1. Effect of soaking time on the grain growth

Figure 1 presents the microstructures of 15Cr-22Ni iron-base superalloy with different niobium contents after hot forging. The grains of significantly varying sizes in the microstructures after hot forging were observed as shown in Figure 1. The grains of the as-forged superalloy V1 are much larger than those of the superalloys V2 and V3. The average grain sizes of as-forged superalloys V1, V2 and V3 are 55, 15 and 15 μm, respectively.

**Table I. Chemical Compositions of 15Cr-22Ni Iron-Base Superalloys (Mass Pct)**

Superalloy No.	C	Si	Mn	Mo	Ti	Cr	Ni	Al	Nb
V1	0.024	0.5	0.75	2.5	0.10	14.2	22	0.11	0.64
V2	0.027	0.5	0.75	2.5	0.11	14.7	22	0.15	1.00
V3	0.026	0.5	0.75	2.5	0.10	14.8	22	0.13	1.40

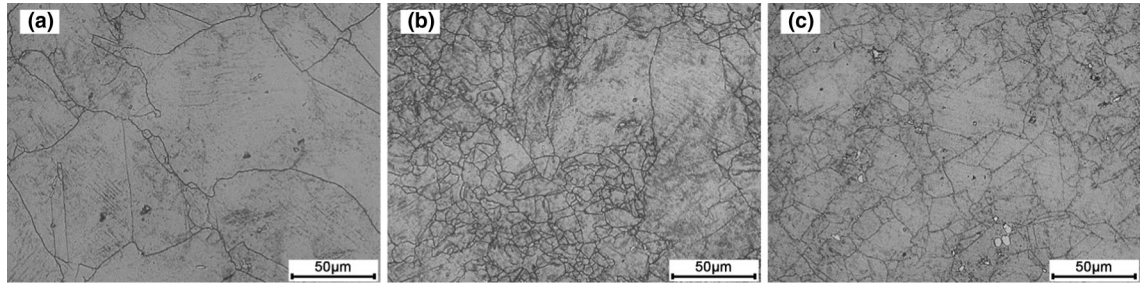


Fig. 1—Optical micrographs of 15Cr-22Ni iron-base superalloy after hot forging: (a) V1, (b) V2, (c) V3.

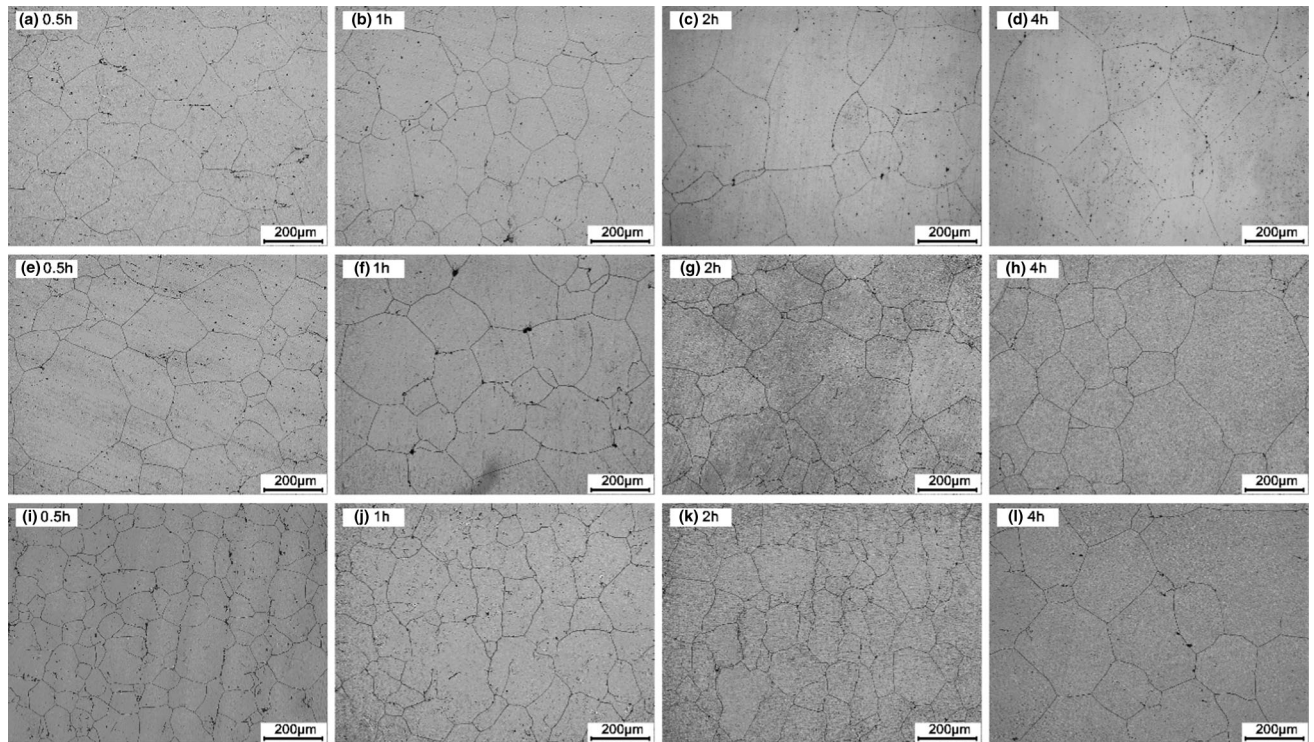


Fig. 2—Optical micrographs of 15Cr-22Ni iron-base superalloy after the solution at 1473 K (1200 °C) for different soaking times: (a) through (d) V1, (e) through (h) V2, (i) through (l) V3.

Figure 2 shows the microstructures of 15Cr-22Ni iron-base superalloy with different niobium contents after solution treatment at 1473 K (1200 °C) for different soaking times. The size of austenite grains increases and amount of fine grains decreases with the increase in the soaking time, as shown in Figure 2. Meanwhile, the equiaxed microstructure is achieved after the solution at various holding temperatures and

soaking time. Note that a greater diversity and more uneven distribution of grain size were observed at longer soaking time.

Figure 3 shows the statistics of the average austenite grain size of 15Cr-22Ni iron-base superalloy after solution treatment at different holding temperatures and soaking times. For each superalloy, the average austenite grain sizes nearly linearly increase as the

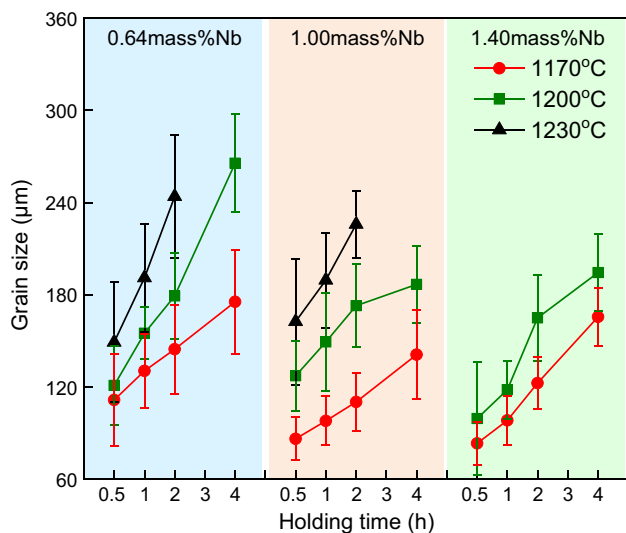


Fig. 3—Variation of the grain size of 15Cr-22Ni iron-base superalloy after the solution at different holding temperatures and soaking times.

soaking time is increased from 0.5 to 4 hours at various solution temperatures, as shown in Figure 3. This is consistent with the microstructure observation shown in Figure 2. The average austenite grain sizes of the superalloy with different niobium contents are increased by > 60 pct with increasing the soaking time from 0.5 to 4 hours at all solution temperatures, except for the grain size of superalloy V2 at solution temperature of 1473 K (1200 °C) (increased by only 46.8 pct). The migration of grain boundaries leads to the gradual growth of the grains with extending the soaking time. The grain grows up normally when holding for 0.5–1 hours at the holding temperature of 1473 K (1200 °C).

However, there is a transition in grain growth model from normal to abnormal when extending the soaking time to 2 hours at 1473 K (1200 °C). Both coarsened and fine austenite grains are observed after the solution is held for 4 hours at different soaking temperatures, indicating that the growth rate of fine grains is smaller than that of coarsened grains. Figure 3 shows that the grain size of superalloy V1 is larger than that of superalloys V2 and V3 after the solution treatment at a given holding temperature and soaking time. Correlating the grain growth during both the thermal cycle of hot forging and holding of the solution indicates that niobium addition inhibits the grain growth of 15Cr-22Ni iron-base superalloy, and the grain growth rate of high-Nb 15Cr-22Ni iron-base superalloy is lower than that of the low-Nb superalloy.

## 2. Effect of solution temperature on the grain growth

Figure 4 shows the microstructure of 15Cr-22Ni iron-base superalloy with different niobium contents at different solution temperatures and the soaking time of 2 h. Obvious coarsening of the austenite grains was observed in the solution temperature range of 1443 K (1170 °C) to 1503 K (1230 °C). The degree of grain coarsening increases with increasing the solution

temperature. The increase in the grain size with increasing the solution temperature indicates that grain boundary migration occurs at elevated temperatures because of the increase in the solute diffusion rate. The austenite grain growth is inhibited by the pinning force brought by a large amount of nano-sized NbC particles along the grain boundaries. NbC precipitates would be fully dissolved when the solution temperature exceeds the dissolution temperature of NbC thermodynamically. Both the dissolution and coarsening of NbC particles would reduce the pinning force and result in abnormal grain growth. Meanwhile, the abnormal grain growth takes place at the expense of fine grains, leading to a decrease in the number of fine grains and an increase in the amount of coarsened grains. Therefore, both normal and abnormal grain growths occur at elevated temperatures, as shown in Figures 4(d), (e), and (f). Normal and abnormal growth of grains would lead to unimodal and bimodal distribution of grain size, respectively.<sup>[23]</sup>

According to the criterion proposed by Rios<sup>[23,24]</sup> and Novikov<sup>[25]</sup> for assessing the normal and abnormal growth of grains, the normal grain growth (NGG) and abnormal grain growth (AGG) are marked in the optical micrographs, as shown in Figures 4(d) through (f). Abnormal grain growth is dependent on various factors, including solution temperature, soaking time, precipitates and transient grain size. The discussion on this aspect is presented in Section III-C.

Figure 5 shows the grain size distribution of 15Cr-22Ni iron-base superalloy after solution at the holding temperature of 1443 K (1170 °C) and 1473 K (1200 °C) for a soaking time of 2 h. The grain size distribution is mainly in the range of 50 to 150 μm, which exhibits a unimodal distribution (see Figures 5(a), (b) and (c)). This indicates that the austenite grain grows normally at the holding temperature of 1443 K (1170 °C). The amount of grains > 150 μm decreases obviously with the increase in the Nb content. In the case of the solution temperature of 1473 K (1200 °C), the microstructure of mixed grains was observed, which has a feature of bimodal appearance in grain distribution, as shown in Figures 5(d), (e), and (f). Different modes of grain growth contribute to the selective growth of austenite grains.

The temperature at which abnormal grain growth just begins is defined as the temperature of grain coarsening (TGC). The austenite grains of superalloys V1, V2 and V3 become coarse, and their size distribution shows bimodal appearance at the solution temperature of 1473 K (1200 °C) (see Figures 4 and 5). Thus, the grain coarsening temperature (TGC) of the superalloy is taken as 1473 K (1200 °C). Figure 5 also shows that the grain sizes of superalloys V1, V2 and V3 are mainly distributed at around 125, 75 and 100 μm, respectively. Note that the deviation of the grain size distribution range from the average grain size (around 75 μm) of superalloy V2 is smaller than that of superalloys V1 and V3, which is evidence of more even grain sizes of superalloy V2.

Figure 6 presents the FE-SEM backscattered electron (BSE) images and EDS spectra of the precipitates in 15Cr-22Ni iron-base superalloy with 1.00 mass pct Nb before and after solution treatment. The size of NbC

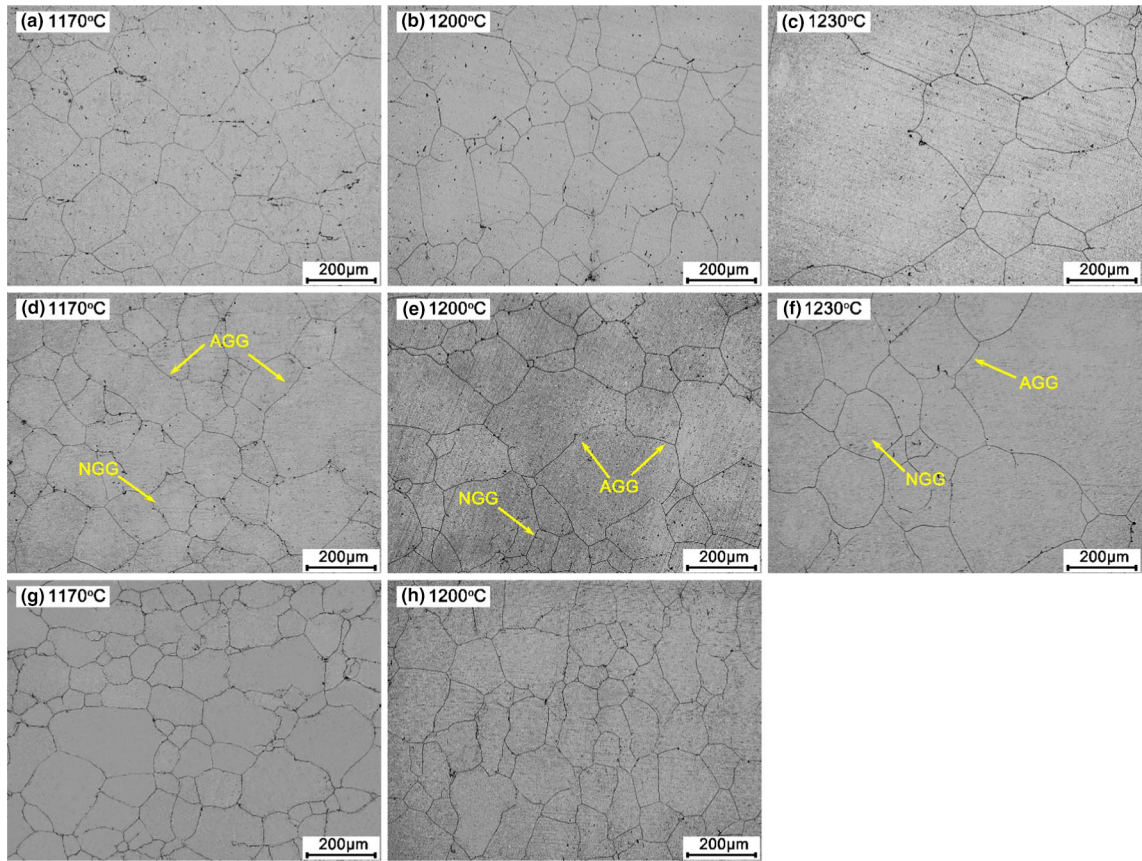


Fig. 4—Optical micrographs of 15Cr-22Ni iron-base superalloy after solution treatment at different temperatures holding for 2 h: (a) through (c) V1, (d) through (f) V2, (g) and (h) V3.

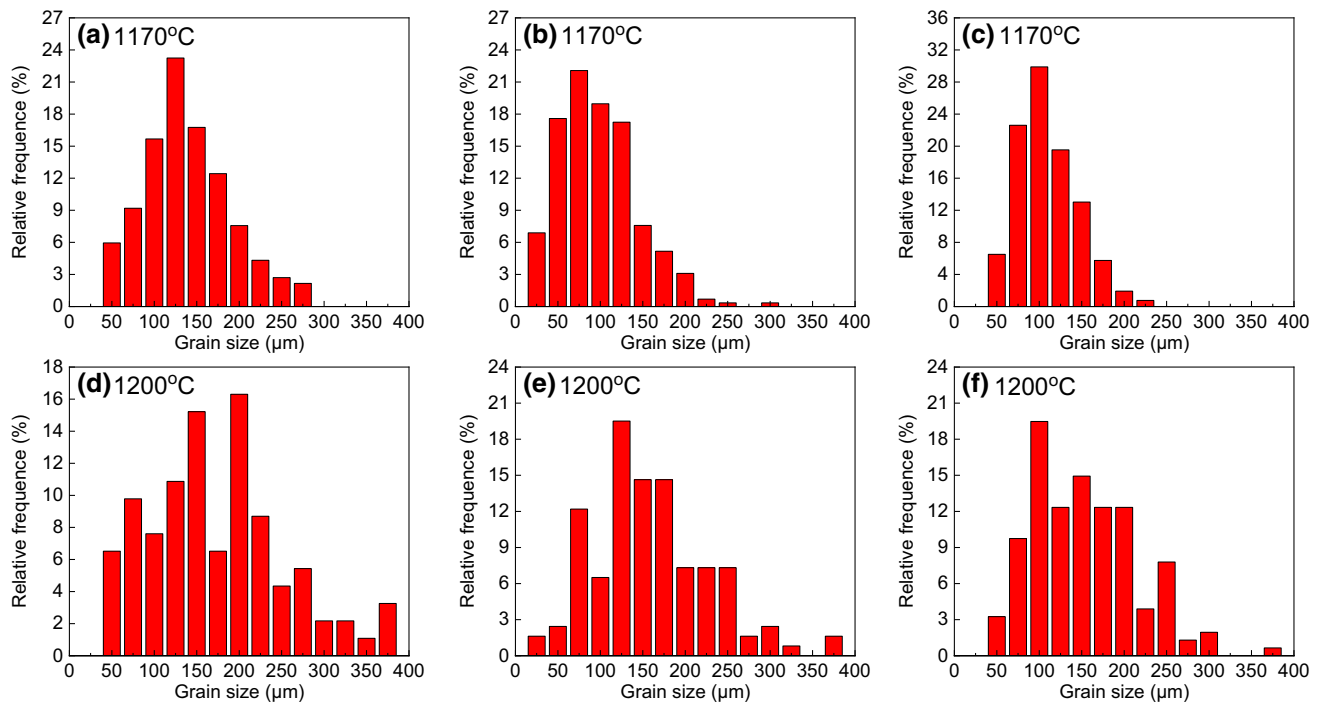


Fig. 5—Grain size distribution of 15Cr-22Ni iron-base superalloy after the solution at 1443 K (1170 °C) and 1473 K (1200 °C) for holding 2 h: (a) and (d) V1, (b) and (e) V2, (c) and (f) V3.

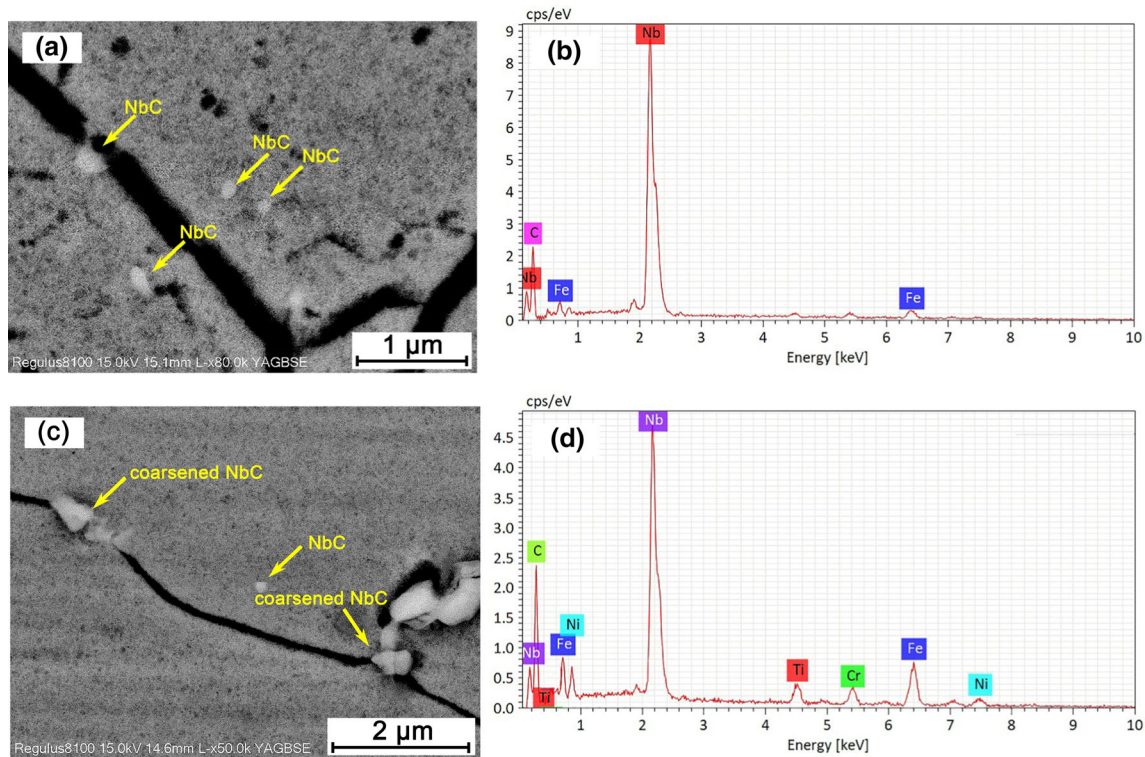


Fig. 6—BSE images and EDS spectra of the precipitates in the superalloy with 1.00 mass pct Nb: (a) and (b) microstructure after hot forging and EDS spectrum of NbC, respectively. (c) and (d) Microstructure after the solution at 1443 K (1170 °C) for 2 hours and EDS spectrum of NbC, respectively.

particles is around 150 nm (see Figure 6(a)). These NbC particles are located along the grain boundaries and play an effective role in pinning of grain boundary migration. As shown in Figure 6(c), a small amount of NbC particles with the size of about 160 nm is found along the grain boundaries after the solution at 1443 K (1170 °C) for 2 h. Furthermore, obviously coarsened NbC particles with the size of about 700 nm are also observed at the grain boundaries. The dissolution and coarsening of NbC particles are greatly dependent on the solution temperatures. It should be noted that few NbC particles are observed in these superalloys after the solution at the holding temperature of 1473 K (1200 °C) and the soaking time of 2 h. The variation of NbC particles sizes with the solution temperatures is in agreement with the change in the grain sizes, as shown in Figure 3.

The pinning force on the fine grains is greater than that on the large grains when the abnormal growth of the grains takes place.<sup>[24]</sup> Consequently, only a few large grains are prone to grow up, dominating the grain growth process. Large grains have a higher growth rate compared with that of the fine grains. Meanwhile, the differences in the growth rates of large grains and their neighbors would further enhance the differences in the grain sizes and grain growth rates.<sup>[24]</sup> The number of the abnormally grown grains in different unit areas is largely dependent on the probability factor because of the inhomogeneity of grain size distribution, which results in a difficulty in quantitatively controlling the grain growth in unit area.<sup>[23]</sup> However, increasing the Nb

content of the 15Cr-22Ni iron-base superalloy promotes the precipitation of more fine NbC particles in unit area. These fine NbC particles would provide a strong pinning force on the grain boundaries and consequently inhibit the grain growth and improve the grain degree.

## B. Phase Precipitation and Solubility Product of NbC

### 1. Phase precipitation of 15Cr-22Ni iron-base superalloy

Figure 7 shows the equilibrium phase precipitation of superalloys V1, V2 and V3 calculated with Thermo-Calc software (TCFE8 database). The dissolution temperature of NbC precipitates increases from 1530 K (1257 °C) to 1540 K (1267 °C) when the niobium content of the superalloy is increased from 0.64 mass pct to 1.00 mass pct, and the dissolution temperature decreases slightly to 1537 K (1264 °C) with further increasing of the niobium content up to 1.40 mass pct. NbC precipitates in superalloy V1 are more prone to dissolve in superalloy matrix than that in superalloys V2 and V3 because of the lower dissolution temperature, as shown in Figure 7. It is noted that NbC precipitates would still present even though these superalloys were solution treated at 1443 K (1170 °C), 1473 K (1200 °C) and 1503 K (1230 °C).

Figure 7 shows that the dissolution temperature of Laves phase increases from 1113 K (860 °C), 1233 K (960 °C) to 1323 K (1050 °C) with the increase in the niobium content from 0.64 mass pct, 1.00 mass pct to

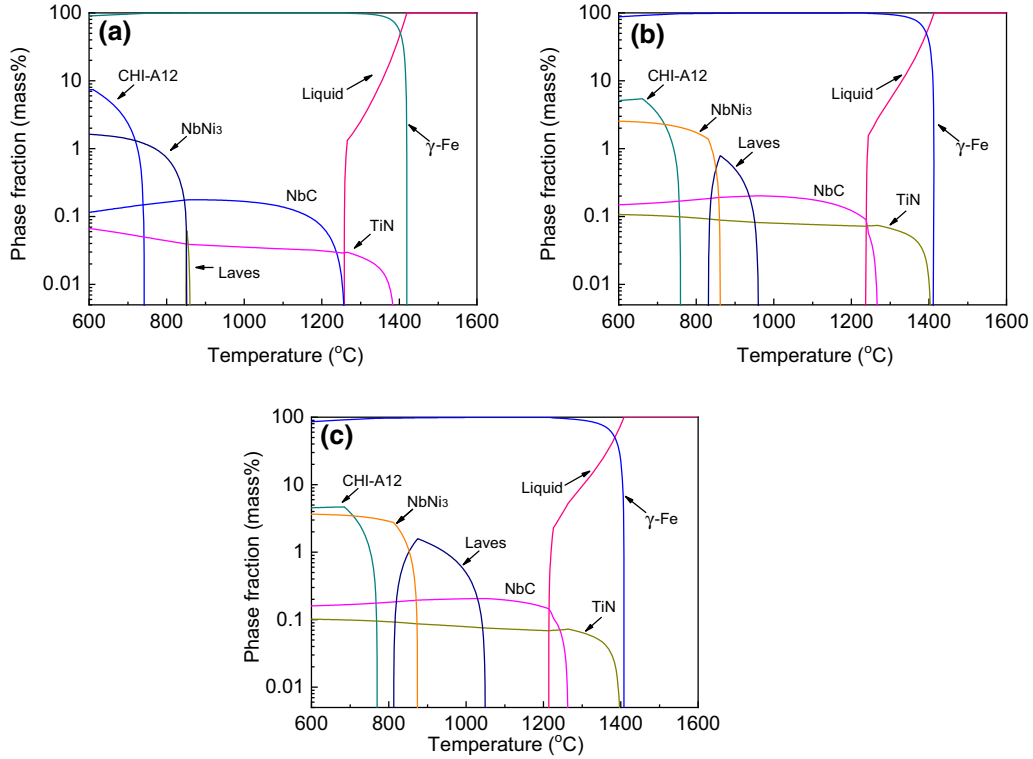


Fig. 7—Phase equilibrium precipitation of 15Cr-22Ni iron-base superalloy calculated with Thermo-Calc: (a) V1, (b) V2, (c) V3.

1.40 mass pct, respectively. Laves phase particles were not fully dissolved during the homogenization at 1433 K (1160 °C) for 3 hours prior to hot forging because of the limitation of the dissolution kinetics (the quantity statistics of Laves phase is shown in Fig. 18). Niobium is one of the Laves phase-forming elements. There is a competitive correlation between niobium-containing Laves phase and NbC precipitates during their precipitation and dissolution.<sup>[26]</sup> Consequently, simultaneous dissolution of NbC and niobium-containing Laves phase in the solution process has a great influence on the mechanical properties of the superalloy.

## 2. Solubility product of NbC

NbC particles would precipitate once the concentration product of Nb and C exceeds the equilibrium solid solubility product. Nb and C in solute state in superalloy are denoted as [Nb] and [C]. The solid solubility product of NbC in austenite can be expressed as follows.<sup>[22]</sup>

$$\log\{[\text{pct Nb}] \times [\text{pct C}]\} = 3.04 - 7290/T \quad [1]$$

The interaction coefficients (shown in Table II) are introduced to modify Eq. [1] in combination with the Wagner formula,<sup>[27]</sup> in consideration of the influence of solute elements on the dissolution of NbC precipitates. Thus, Eq. [1] can be rewritten as Eq. [2].

$$\log\{[\text{pct Nb}] \times [\text{pct C}]\} = 3.45 - 8098/T - (0.0078 + 118.9/T) \times [\text{pct Nb}] \quad [2]$$

Table II. Interaction Parameters in Austenite<sup>[28]</sup>

$i, j$	$e_j^i = A + B/T$	
	$A$	$B$
Mn, Nb	203.57	- 305033
Mn, C	—	- 5070
Si, Nb	- 44.91	77265
Si, C	4.84	7370
Nb, Nb	- 2	—
Nb, C	—	- 66257
C, C	—	8890
Mo, C	3.86	- 17870

The solubility product [pct Nb] × [pct C] calculated using Eq. [2] is plotted as a function of the solution temperatures, as shown in Figure 8. The measured contents of Nb and C in the superalloys are also presented (points V1, V2 and V3) in Figure 8. It can be seen that the concentration products of measured Nb and C contents in the superalloys are higher than the solid solubility product of NbC at different temperatures calculated using Eq. [2]. The deviation of the measured concentration products from the calculated solid solubility product of NbC becomes larger with the increase in the Nb content. The points above the solid solubility product curves indicate that [Nb] and [C] in the superalloys are in the supersaturation state. The deviation of points V1, V2 and V3 from solid solubility product of NbC represents the supersaturation degree of

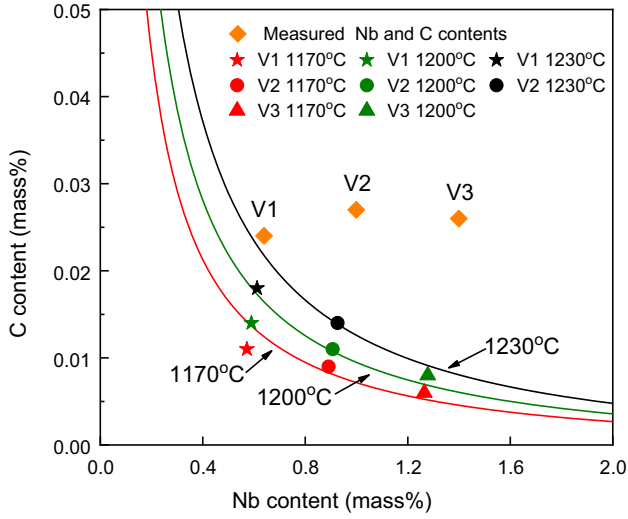


Fig. 8—Relationship between the solubility product of NbC and solution temperatures. Notes: The contents of [Nb] and [C] at different solution temperatures were calculated with Thermo-Calc software (TCFE8 database).

[Nb] and [C], which is the driving force for the precipitation of NbC.<sup>[26]</sup> Therefore, more NbC particles would precipitate with the increase in the niobium contents of the superalloys. As shown in Figure 8, the calculated solubility of NbC in austenite matrix linearly decreases as the solution temperature is decreased.

The equilibrium concentrations of [Nb] and [C] for NbC formation at 1443 K (1170 °C), 1473 K (1200 °C) and 1503 K (1230 °C) calculated with Thermo-Calc are listed in Table III. Note that the concentration products of [Nb] and [C] calculated with Thermo-Calc are in accordance with the solubility product curves of the superalloys V2 and V3, whereas the calculated concentration product is lower than that calculated using Eq. [2] for superalloy V1. The thermodynamic calculation of phase equilibrium precipitation with Thermo-Calc and EDS analysis show that the NbC precipitates in superalloys V1, V2 and V3 contain about 17 atom pct, 11 atom pct and 1 atom pct of titanium, respectively. (Nb,Ti)C is simplified as NbC in the calculation of equilibrium solubility product [pct Nb] × [pct C] using Eq. [2] in view of the low titanium content. This simplification gives rise to the deviation between the concentration products of [Nb] and [C] calculated with Thermo-Calc ((Nb,Ti)C in the calculation) and equilibrium solubility product [pct Nb] × [pct C] using Eq. [2] in superalloy V1, as shown in Figure 8.

### C. Model of Precipitate and Austenite Grain Growth

#### 1. Model of precipitate growth kinetics

Ostwald ripening effect occurs when the diffusivity of solute atoms is high, and the amount and compositions of precipitates are stable.<sup>[29]</sup> The ripening effect induces the large precipitates to absorb the small precipitates continuously and grow up, consequently resulting in the

decrease of the amount of the precipitates and increase in their size.<sup>[30,31]</sup> The large precipitates cannot serve an effective pinning effect on the migration of grain boundaries. Lifshitz and Slyozov<sup>[32]</sup> proposed a kinetic model (expressed as Eq. [3]) for describing the coarsening of second-phase particles.

$$r^3 - r_0^3 = \frac{8\sigma V D t C_s}{9RT} \quad [3]$$

where  $r_0$  is the initial radius of the particle,  $r$  is the particle radius at the soaking time  $t$ ,  $\sigma$  is the interface energy (the interface energy between NbC and austenite in this article),  $V$  is the molar volume of the particles,  $D$  is the diffusion coefficient of the solute atom (referred to niobium diffusion in austenitic matrix),  $C_s$  is the equilibrium concentration of solute atom niobium in the matrix,  $R$  is the gas constant, and  $T$  is the absolute temperature. The parameters used in Eq. [3] are listed in Table IV.

The average size of NbC particles in superalloy V2 after hot forging is around 150 nm (see Fig. 6(a)). The initial radius of NbC particles  $r_0$  is taken as 75 nm in superalloy V2 for calculating the coarsening of NbC particles using Eq. [3]. The coarsened size of NbC is calculated to be 766 nm using Eq. [3], in combination with the solution temperature 1443 K (1170 °C), the soaking time 2 hours and the equilibrium concentration of solute niobium in matrix 0.87 at 1443 K (1170 °C). The calculated result is consistent with the measured size of coarsened NbC particles (around 700 nm, see Fig. 6(c)). The coarsening and dissolution of NbC particles have taken place at the solution temperature 1443 K (1170 °C) as shown in Figures 6 and 8, both of which weaken the pinning force of NbC particles on grain boundaries. Equation [3] shows that the increase in both the temperature and the soaking time would lead to the coarsening of the second-phase particles, and the increase in the niobium content of the superalloy would enhance the coarsening degree of NbC particles.

#### 2. Kinetics of grain growth

The grain growth is the result of the combined action of the pinning force of the second particles on the grain boundaries  $\Delta F_{\text{drag}}$  and the driving force of grain growth  $\Delta F$ .<sup>[34]</sup> The relationship among the pinning force  $\Delta F_{\text{drag}}$ , the particle radius  $r$  and the particle volume fraction  $f$  in microstructure can be expressed as<sup>[34]</sup>

$$\Delta F_{\text{drag}} = \gamma_B Z = 1.5 \gamma_B \frac{f}{r} \quad [4]$$

where  $\gamma_B$  is the interface energy per unit area of grain boundary.

The decrease in the interface energy is the driving force for grain growth.<sup>[34,35]</sup> The relationship between the driving force of grain growth  $\Delta F$  and the grain size  $d$  is shown in Eq. [5].

$$\Delta F = 2 \frac{\gamma_B}{d} \quad [5]$$



**Table III. Mass Fraction of NbC and the Contents of [Nb] and [C] in the Superalloys at Different Solution Temperatures Calculated with Thermo-Calc (Mass Pct)**

Superalloy No.	1503 K (1230 °C)			1473 K (1200 °C)			1443 K (1170 °C)		
	Mass Fraction	[Nb]	[C]	Mass Fraction	[Nb]	[C]	Mass Fraction	[Nb]	[C]
V1	0.039	0.605	0.02	0.072	0.576	0.017	0.097	0.553	0.016
V2	0.097	0.913	0.017	0.122	0.890	0.014	0.143	0.870	0.010
V3	0.097	1.313	0.014	0.154	1.261	0.012	0.170	1.247	0.008

**Table IV. Parameters Included in the Calculation Using Eq. [3]**

Parameter	Value <sup>[33]</sup>	Unit
$r_0$	$7.5 \times 10^{-8}$	m
$\sigma$	$1.3435 - 6.054 \times 10^{-4}T$	J/m <sup>2</sup>
$V$	$1.375 \times 10^{-5}$	m <sup>3</sup> /mol
$D$	$8.3 \times 10^{-5} \times \exp(-266500/RT)$	m <sup>2</sup> /s
$t$	7200	s
$C_s$	0.87*	mass pct
$R$	8.314	J/mol · K <sup>-1</sup>
$T$	1443	K

\*This value is cited from Table III.

The abnormal growth of grains occurs once the driving force of grain growth  $\Delta F$  is greater than the pinning force of the second particles on the grain boundaries  $\Delta F_{\text{drag}}$ . In this case where  $\Delta F$  is equal to  $\Delta F_{\text{drag}}$ , Eq. [6] can be obtained by combining Eqs. [4] and [5].

$$2 \frac{\gamma_B}{d} = 1.5 \gamma_B \frac{f}{r} \quad [6]$$

The critical grain size  $d_{\text{critical}}$  of abnormal growth can be obtained from Eq. [7].

$$d_{\text{critical}} = \frac{4r}{3f} \quad [7]$$

Gladman *et al.*<sup>[36]</sup> modified Eq. [7] by combining the force of grain boundary migration and the pinning force in the process of grain coarsening and obtained the following equation:

$$d_{\text{critical}} = \frac{\pi}{6} \left( \frac{3}{2} - \frac{2}{Z} \right) \frac{r}{f} \quad [8]$$

The size of the precipitates increases in the coarsening process, and the equilibrium volume fraction of the precipitates is constant at a given temperature.<sup>[30,31]</sup> Thus, the pinning effect contributed by these precipitates on the grain boundaries would be lowered. The migration of the grain boundaries with a high free energy leads to the grain growth when the pinning force supplied by the precipitates is decreased. The migration rate of the grain boundaries is proportional to the driving force of grain growth as expressed in Eq. [9].<sup>[37]</sup>

$$v = M\Delta F \quad [9]$$

where  $v$  is the migration rate of the grain boundary, and  $M$  is the constant of effective boundary mobility.

The growth rate can also be expressed as a function of the grain size and time, as shown in Eq. [10].

$$v = \frac{1}{2} \frac{dd}{dt} \quad [10]$$

where  $\frac{dd}{dt}$  is the growth rate of austenite grain. The migration rate is transformed into the Arrhenius-type equation. Equation [11] can be obtained by combining Eqs. [5], [9] and [10].

$$\frac{dd}{dt} = \frac{2M_0\gamma_B}{d} \exp\left(-\frac{Q}{RT}\right) \quad [11]$$

The growth rate of the grains can be determined using Eq. [11]. The growth rate of grain increases with the increase in the temperature, whereas the growth rate would be inhibited by the grain size. It suggests that the grains would not grow up continually over time, and the growth rate of the grains becomes lower as they reach a certain size.

### 3. Mathematical model of grain growth

The aforementioned experimental results and analysis demonstrate that both the solution temperature and soaking time play an important role on the grain growth of 15Cr-22Ni iron-base superalloys. Beck *et al.*<sup>[38]</sup> proposed a model to describe the normal growth of the austenite grains, as expressed in Eq. [12].

$$d - d_0 = kt^m \quad [12]$$

where  $k$  is a grain growth rate constant, and  $m$  is the grain growth exponent.

However, the grain growth model (*i.e.*, Eq. [12]) proposed by Beck *et al.*<sup>[38]</sup> cannot be used to predict the grain growth. Later, Anelli<sup>[39]</sup> developed a model to predict the austenite grain size during the austenite grain growth. By modifying the model proposed by Anelli<sup>[39]</sup> in consideration of the influence of initial grain size, Raghunathan<sup>[40]</sup> established a model (see Eq. [13]) to describe and predict the austenite grain growth.

$$d - d_0 = At^m \exp(-Q/RT) \quad [13]$$

where  $d_0$  and  $d$  are the initial grain size and average grain size ( $\mu\text{m}$ ),  $A$  is a constant for a given steel composition and processing condition,  $m$  is the exponent of grain growth time,  $Q$  is the activation energy of grain growth (J/mol), and  $R$  is the gas constant (8.314

J/mol·K<sup>-1</sup>). Taking the natural logarithm of Eq. [13], the following equation is obtained.

$$\ln(d - d_0) = \ln A + m \ln t - Q/RT \quad [14]$$

The partial derivatives of Eq. [14] can be expressed as Eqs. [15] and [16] at a given soaking time and solution temperature.

$$Q = -R \frac{\partial[\ln(d - d_0)]}{\partial(1/T)} \Big|_{t=\text{constant}} \quad [15]$$

$$m = \frac{\partial[\ln(d - d_0)]}{\partial(\ln t)} \Big|_{T=\text{constant}} \quad [16]$$

The activation energy of grain growth  $Q$  and the exponent of grain growth time  $m$  can be obtained from the slope of the linear fitted plot of  $\ln(d - d_0)$  versus  $1000/T$ , and  $\ln(d - d_0)$  vs  $\ln t$ , as shown in Figures 9 and 10. The values of  $Q$  for 15Cr-22Ni iron-base superalloy V1, V2 and V3 are calculated to be 210.477, 239.636 and 268.796 kJ/mol, respectively. The values of  $m$  are determined as 0.458, 0.268 and 0.381 for 15Cr-22Ni iron-base superalloy V1, V2 and V3, respectively.

The parameter  $A$  can be obtained by substituting  $Q$  and  $m$  into Eq. [14]. The values of parameter  $A$  are calculated to be  $6.86 \times 10^7$ ,  $4.40 \times 10^9$  and  $1.79 \times 10^{10}$  for 15Cr-22Ni iron-base superalloy V1, V2 and V3, respectively. The model proposed by Raghunathan<sup>[40]</sup> for describing and predicting the austenite grain growth of 15Cr-22Ni iron-base superalloy V1, V2 and V3 can be expressed as Eqs. [17] through [19], respectively.

$$d_1 = 55 + 6.86 \times 10^7 \times t^{0.458} \exp\left(\frac{-210477}{RT}\right) \quad [17]$$

$$d_2 = 15 + 4.40 \times 10^9 \times t^{0.268} \exp\left(\frac{-239636}{RT}\right) \quad [18]$$

$$d_3 = 15 + 1.79 \times 10^{10} \times t^{0.381} \exp\left(\frac{-268796}{RT}\right) \quad [19]$$

Figure 11 shows the change of the grain size of 15Cr-22Ni iron-base superalloy at different solution temperatures and soaking times predicted by the model proposed by Raghunathan.<sup>[40]</sup> The measured average grain size is also presented in Figure 11 for comparison.

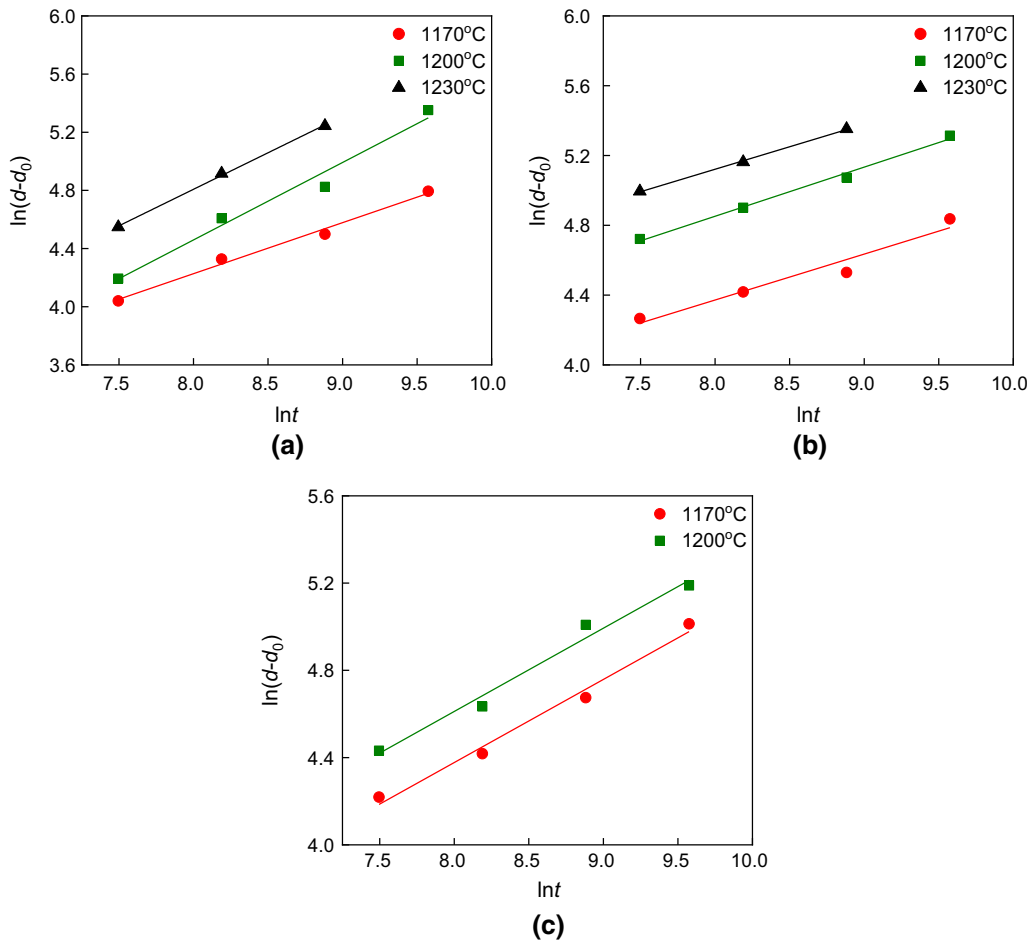


Fig. 9—Plots of  $\ln(d - d_0)$  versus  $\ln t$  at different solution temperatures: (a) superalloy V1, (b) superalloy V2 and (c) superalloy V3.

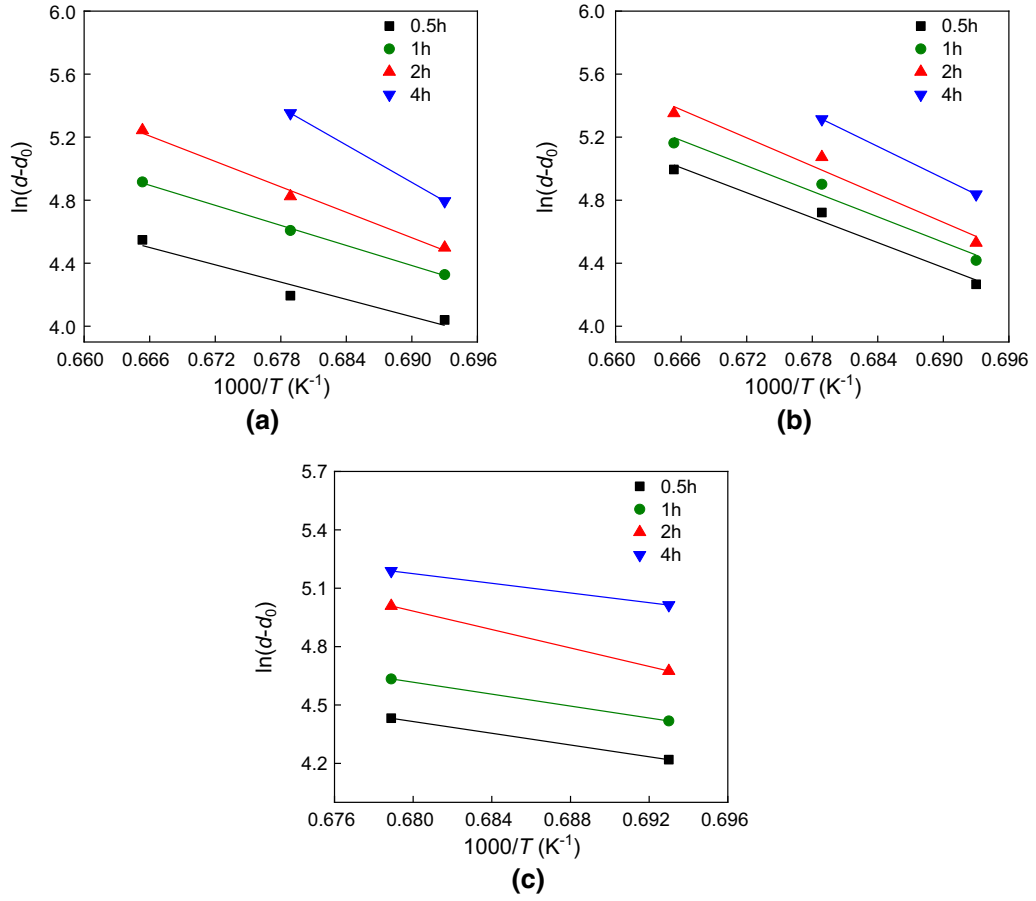


Fig. 10—Plots of  $\ln(d - d_0)$  versus  $1000/T$  at different soaking times: (a) superalloy V1, (b) superalloy V2 and (c) superalloy V3.

The predicted grain size is in good agreement with the measured grain size as shown in Figure 11. It suggests the good availability of the model proposed by Raghunathan<sup>[40]</sup> in predicting the grain growth of 15Cr-22Ni iron-base superalloy. To determine the prediction accuracy of the model proposed by Raghunathan,<sup>[40]</sup> a comparison of the predicted grain size and measured average grain size at different solution temperatures is shown in Figure 12. Meanwhile, the values of mathematical errors, *i.e.*, correlation coefficient ( $R$ ) and represented average absolute relative error ( $AARE$ ), are calculated using Eq. [20] and [21].

$$R = \frac{\sum_{i=1}^N (E_i - \bar{E})(P_i - \bar{P})}{\sqrt{\sum_{i=1}^N (E_i - \bar{E})^2 \sum_{i=1}^N (P_i - \bar{P})^2}} \quad [20]$$

$$AARE = \frac{1}{N} \sum_{i=1}^N \left| \frac{E_i - P_i}{E_i} \right| \times 100\text{pct} \quad [21]$$

where  $E_i$  is the measured average grain size,  $P_i$  is the predicted grain size,  $\bar{E}$  and  $\bar{P}$  represent the mean values of  $E_i$  and  $P_i$ , respectively. The values of  $R$  were calculated to be 0.992, 0.987 and 0.950 for superalloys V1, V2 and V3, respectively. The values of  $AARE$  are determined to

be 4.43 pct, 4.70 pct and 9.56 pct, respectively. The calculated values of mathematical errors suggest that the model proposed by Raghunathan<sup>[40]</sup> is applicable to predict the grain size growth of 15Cr-22Ni iron-base superalloys.

To further reveal the effect of the Nb content on austenite grain growth, the parameters  $\ln A$ ,  $m$  and  $Q$  are expressed as a function of the niobium contents in the superalloy, as shown in Figure 13. Equations [22] through [24] are obtained by nonlinearly fitting the parameters  $\ln A$ ,  $m$  and  $Q$  with the total niobium content of the superalloys  $[\text{pct Nb}]_{\text{total}}$ , respectively.

$$\ln A = 24.17 - 45.67 \exp(-3.138 \times [\text{pct Nb}]_{\text{total}}) \quad [22]$$

$$m = 1.066 \times [\text{pct Nb}]_{\text{total}}^2 - 2.276 \times [\text{pct Nb}]_{\text{total}} + 1.478 \quad [23]$$

$$Q = 76665 \times [\text{pct Nb}]_{\text{total}} + 161950 \quad [24]$$

The grain growth generally is caused by the migration of grain boundaries, which is a thermal activation process and dependent on the activation energy of grain growth.<sup>[20]</sup> The amount of NbC precipitates increases with the increase in the niobium contents of 15Cr-22Ni

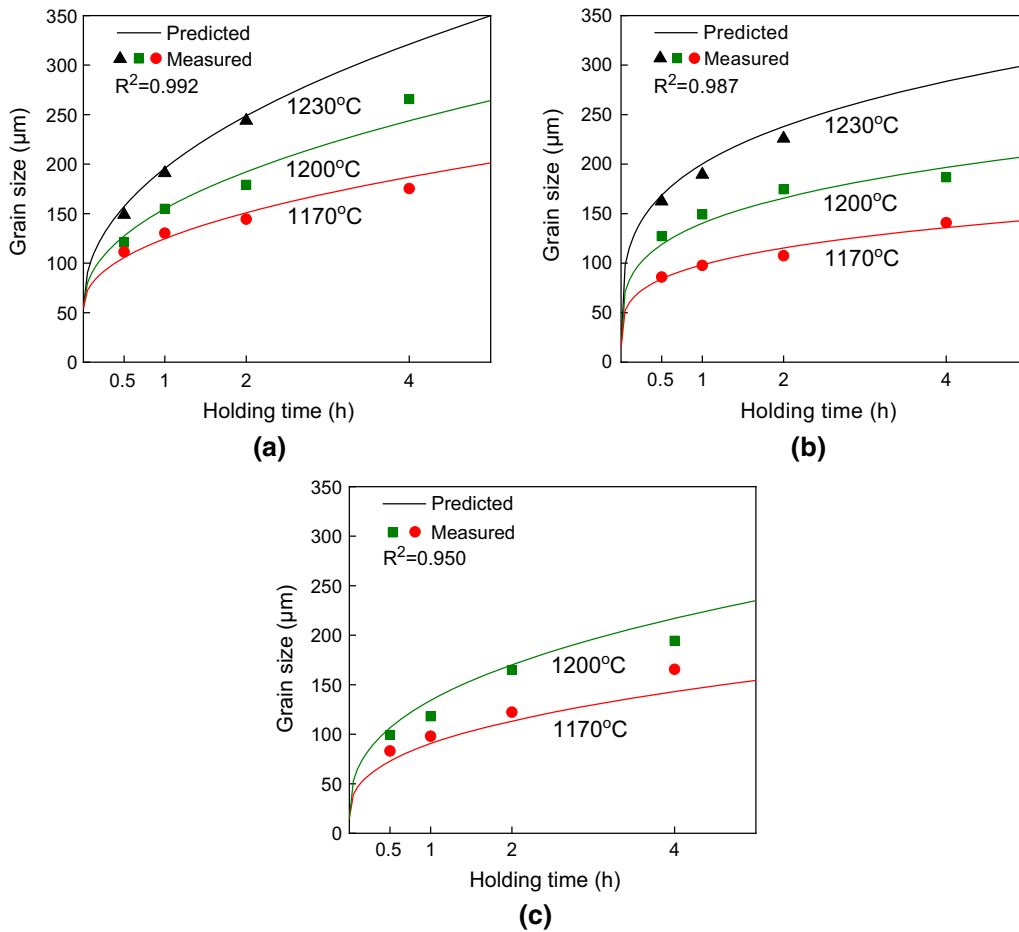


Fig. 11—Change in the grain size predicted by the model proposed by Raghunathan<sup>[40]</sup> and measured average grain size after the solution at different holding temperatures with the soaking time: (a) superalloy V1, (b) superalloy V2 and (c) superalloy V3.

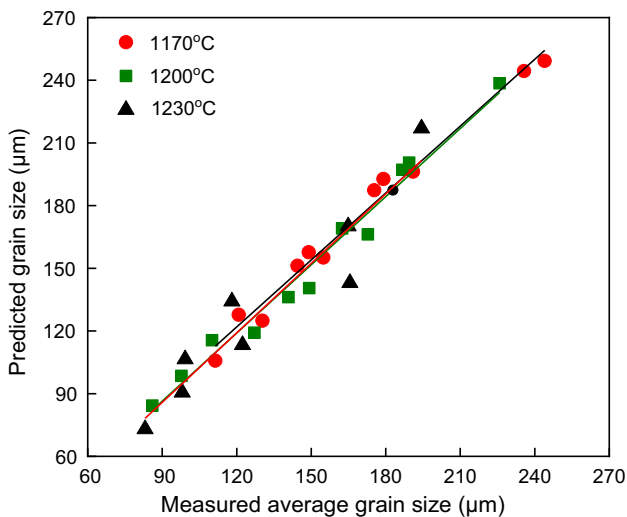


Fig. 12—Comparison of the predicted grain size using the model proposed by Raghunathan<sup>[40]</sup> and measured average grain size at different solution temperatures.

iron-base superalloy. In consideration of the interaction between grain boundaries and precipitates, the coarsening characteristics of the grains are greatly affected by the amount of NbC particles. The migration of the grain boundaries away from the second-phase particles would lead to an increase in the pinning force in local area. Therefore, thermal activation energy  $Q$  increases with the increase in the niobium content. This deduction is supported by the calculated values of  $Q$  (see the values in this section). The present finding is consistent with the result reported by Annan.<sup>[41]</sup> The calculated values of activation energy of grain growth in the superalloys V1, V2 and V3 are roughly close to the activation energy of 225 kJ/mol determined for niobium diffusion along dislocations and grain boundaries in austenitic steel reported by Liu.<sup>[42]</sup> The soaking time exponent  $m$  is closely related to the material properties and the thermal cycle, including the pinning force contributed by second phase precipitates, specimen thickness effect and solute drag effect.<sup>[43]</sup> Therefore, the change in the

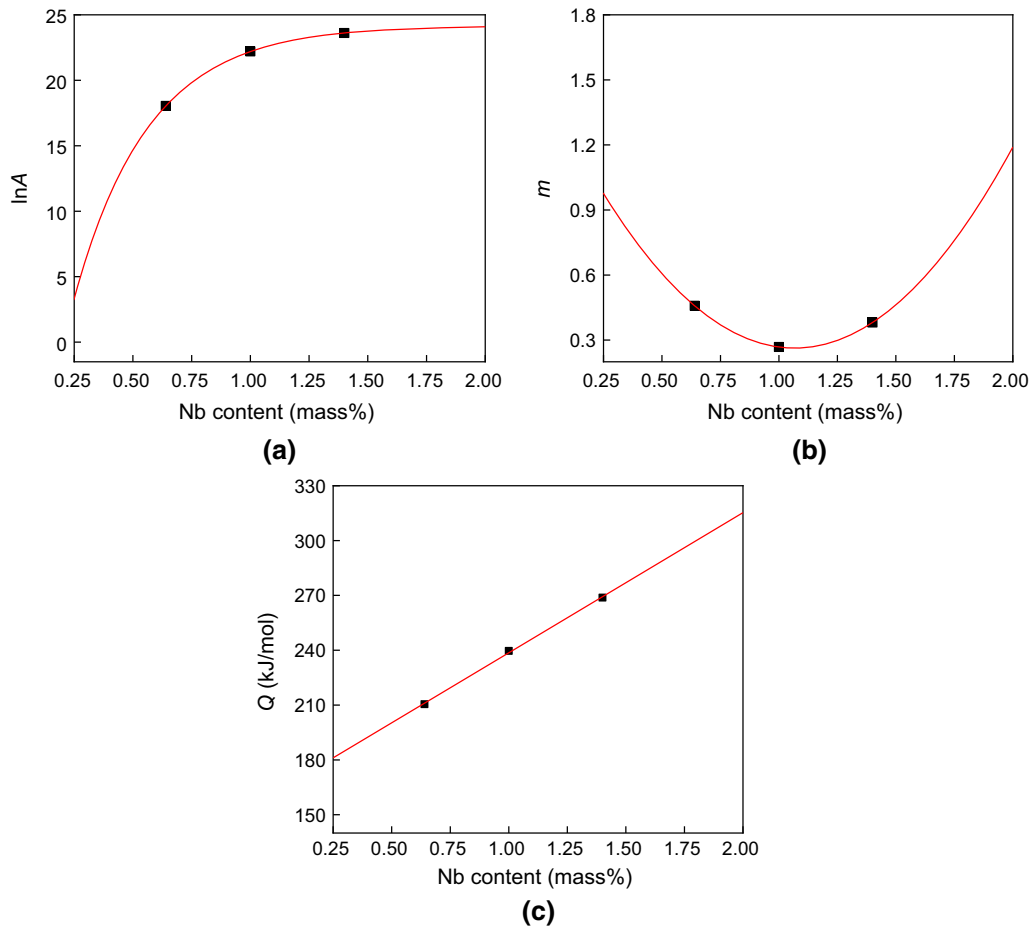


Fig. 13—Fitted plot of the parameters versus the total niobium content of the superalloys: (a) material and processing constant  $A$ , (b) soaking time exponent  $m$  and (c) activation energy  $Q$ .

niobium content would lead to the difference in the values of the soaking time exponent, which could cause the deviation of the predicted grain growth from actual grain growth under different solution conditions.<sup>[41]</sup>

#### D. Eutectic Carbide Dissolution in Solution Treatment

It is more significant to dissolve the large eutectic carbides and achieve even distribution of alloying elements in the solution treatment compared with control of the grain size. The alloying elements could diffuse from the carbides to matrix during the solution treatment. Figure 14 shows the EDS element line scanning across the eutectic carbides after the solution at the holding temperature of 1473 K (1200 °C) and soaking time of 2 hours. An obvious concentration gradient of niobium element near the interface between eutectic NbC precipitate and the superalloy matrix is observed as shown in Figure 14. The niobium content in the matrix nearby eutectic NbC is apparently higher than that away from the eutectic NbC. The morphologies of these eutectic NbC precipitates show transition

layers around their edges next to the superalloy matrix, which is an indication of the partial dissolution of eutectic carbides NbC.

Figure 15 shows the eutectic NbC and Laves phase in superalloy V3 after the solution at 1443 K (1170 °C) for 2 hours. Undissolved Laves phase was only observed in the superalloy V3 after the solution at 1443 K (1170 °C) and different soaking times. EDS element line scanning across a Laves phase precipitate after the solution at 1443 K (1170 °C) for 2 hours is shown in Figure 16. The EDS analysis confirms that Laves phase in 15Cr-22Ni iron-base superalloys is composed of the elements Fe, Cr, Ni, Si, Nb and Mo.

EBSD was employed to confirm the Laves phase according to its crystallographic orientation. Figure 17 shows the EBSD Kikuchi pattern of an undissolved Laves phase particle in superalloy V3 after the solution at 1443 K (1170 °C) for 2 hours. This particle was identified as Fe<sub>2</sub>Nb-type Laves phase by the indexed Kikuchi pattern. According to EDS and EBSD analysis, the Laves phase in 15Cr-22Ni iron-base superalloys was identified as (Fe,Cr,Ni,Si)<sub>2</sub>(Nb,Mo).

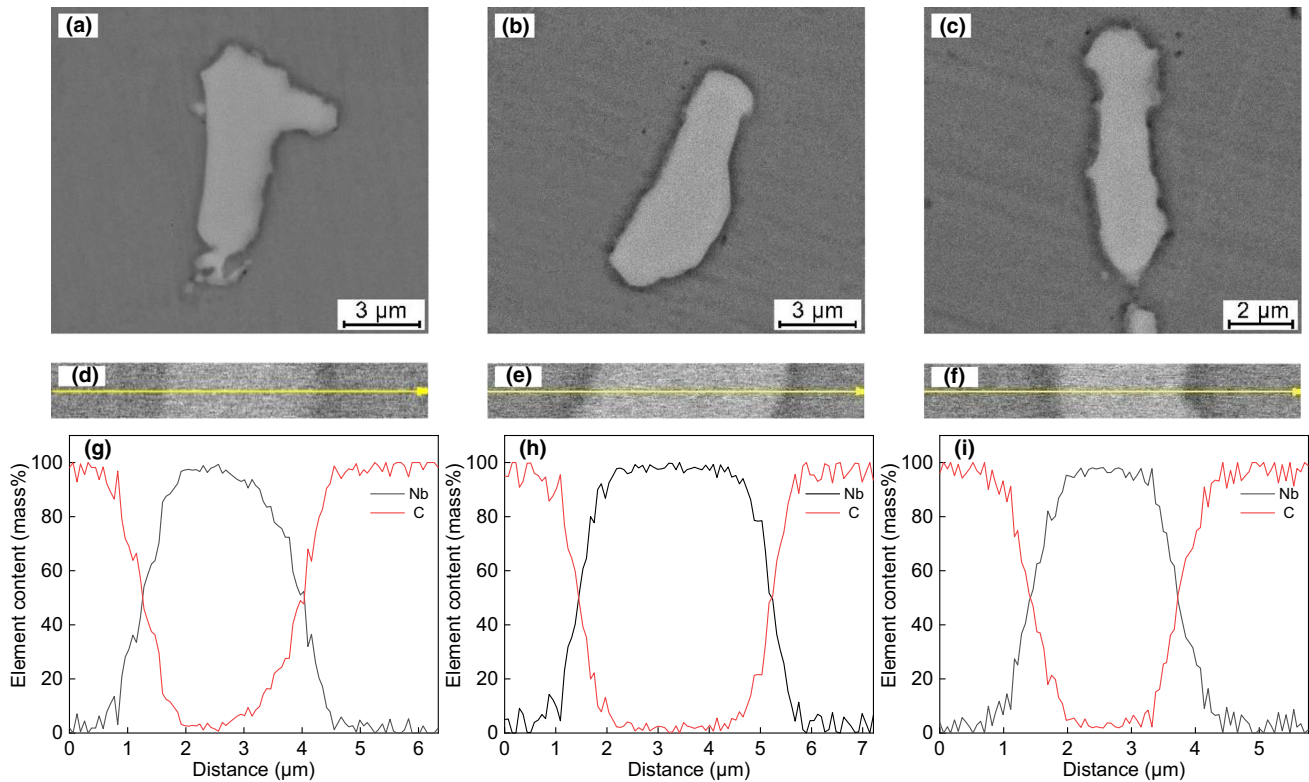


Fig. 14—BSE images and EDS element line scanning of eutectic carbide NbC after the solution at 1473 K (1200 °C) for 2 h: (a) V1, (b) V2, (c) V3. The arrowed lines shown in (d), (e) and (f) indicate the trace of the line scan. (g), (h) and (i) EDS element line scanning results of the eutectic carbide shown in (d), (e) and (f), respectively.

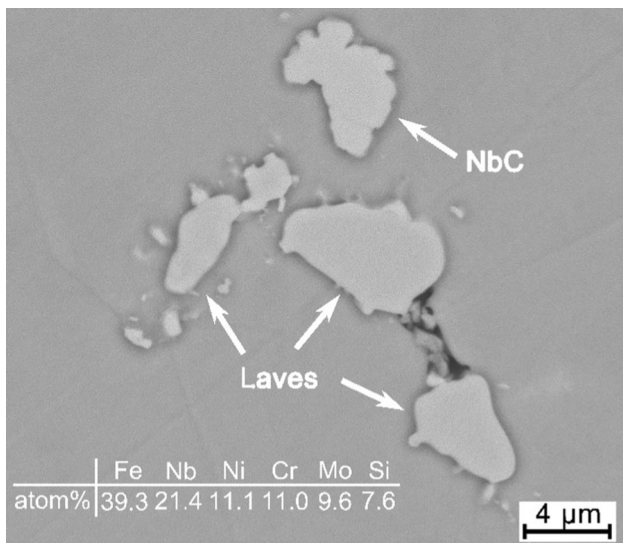


Fig. 15—SEM image and EDS analyzed composition of eutectic carbide NbC and Laves phase in superalloy V3 after the solution at 1443 K (1170 °C) for 2 h.

To quantify the precipitates in the designed superalloy, 30 view fields of SEM images at a magnification of 1500 are randomly selected to calculate the area fraction of eutectic carbides NbC and Laves phase with Image-Pro Plus 6.0 software. Figure 18 shows the statistical results of the area fraction of eutectic carbides

NbC and Laves phases before and after solution treatment at different holding temperatures and soaking time in 15Cr-22Ni iron-base superalloys. As shown in Figure 18, the area fraction of eutectic carbides NbC and Laves phase increases from 0.23 to 0.009 pct in as-forged superalloy V1 to 0.37 and 0.017 pct in as-forged superalloy V2, respectively. However, the area fraction of eutectic carbide NbC decreases to 0.22 pct, whereas the area fraction of Laves phase increases to 0.70 pct in as-forged superalloy V3. At the solution temperatures of 1443 K (1170 °C) to 1503 K (1230 °C), the area fraction of eutectic carbides NbC remains almost unchanged in the case that the soaking time is  $\geq 2$  and 1 hour for the solution of the superalloys V1 and V2, respectively. NbC precipitates will not dissolve when the concentration product of [Nb] and [C] reaches the equilibrium solid solubility product at a given temperature. The concentration product of [Nb] and [C] increases linearly as the temperature is increased from 1443 K (1170 °C) to 1503 K (1230 °C) (see Fig. 8), indicating that the solubility of niobium in the austenite matrix increases with the increase in the temperature and more NbC precipitates can be dissolved.

The area fraction of eutectic carbides NbC in superalloy V3 after the solution at 1473 K (1200 °C) is greater than that after the solution at 1443 K (1170 °C), as shown in Figure 18. As discussed in Section III-B-1, the dissolution of NbC precipitates during solution is in competition with the dissolution of Fe<sub>2</sub>Nb-type Laves phase. According to the equilibrium phase diagrams

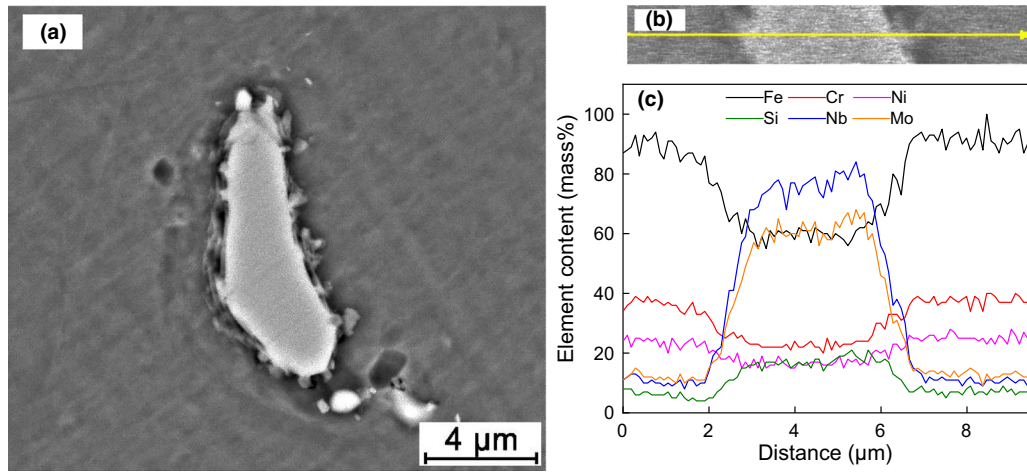


Fig. 16—SEM image of Laves phase in superalloy V3 and EDS element line scanning across a Laves phase particle after the solution at 1443 K (1170 °C) for 2 h. (a) BSE image of Laves phase; (b) the arrowed line indicates the trace of the line scan; (c) EDS element line scanning across the Laves phase shown in (a).

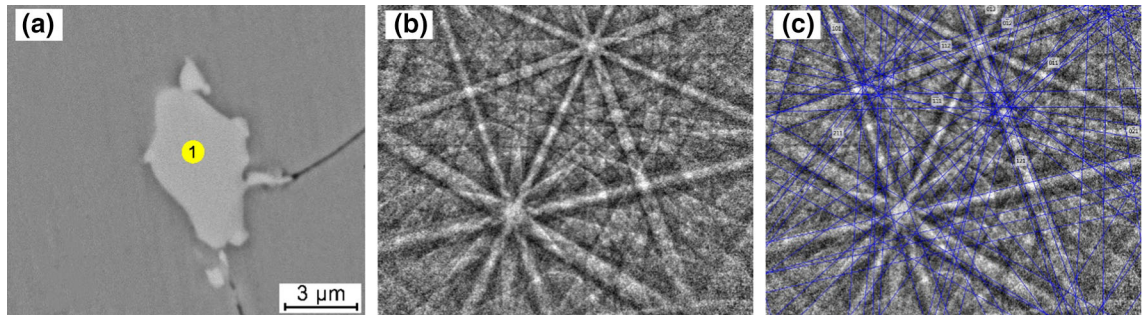


Fig. 17—EBSD identification of Laves phase after the solution at 1443 K (1170 °C) for 2 h: (a) backscattered electron image of Laves phase, (b) raw Kikuchi pattern of Laves phase (point 1 in (a)) and (c) indexed Kikuchi pattern of Laves phase.

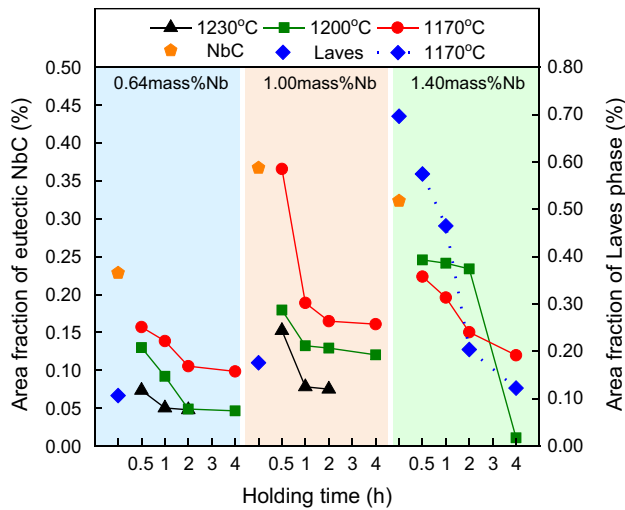


Fig. 18—Area fraction of eutectic carbides NbC and Laves phase before and after the solution at different holding temperatures and soaking times. Note: Laves phase precipitates were only observed in superalloy V3 after the solution at 1443 K (1170 °C) (points connected by dashed line); the points connected by the solid lines represent the change in area fraction of NbC.

shown in Figure 7, Laves phase would dissolve prior to NbC particles during the solution process. Figure 7 also shows that the precipitation quantity and dissolution temperature of Laves phase in superalloy V3 are higher than that in superalloys V1 and V2. Due to the limitation of solute diffusion kinetics during the solution, undissolved Laves phase was observed in superalloy V3 even though the dissolution of NbC precipitates takes place. NbC precipitates dissolve during the solution accompanied by the dissolution of  $Fe_2Nb$ -type Laves phase. The area fraction of eutectic carbides NbC and Laves phase decreases almost linearly with the extension of soaking time at the solution temperature of 1443 K (1170 °C). However, Laves phase is preferential to fully dissolve when the solution temperature is further increased to 1473 K (1200 °C), resulting in the dissolution of a large amount of niobium atoms into the matrix.

As shown in Figure 18, the area fraction of  $Fe_2Nb$ -type Laves phase in superalloy V3 after hot forging is 0.70 pct; 0.13 pct (in area fraction) of Laves phase was dissolved after the solution at 1443 K (1170 °C) for 0.5 h, which would contribute 0.157 mass pct of

soluble niobium to the superalloy matrix. The full dissolution of Fe<sub>2</sub>Nb-type Laves phase after the solution at 1473 K (1200 °C) for 0.5 hour would contribute 0.32 mass pct of soluble niobium to the superalloy matrix. Therefore, the dissolution of part of NbC precipitates would significantly increase the soluble niobium content in the superalloy matrix until the concentration product of [Nb] and [C] reaches the equilibrium solid solubility of NbC. Consequently, the area fraction of eutectic carbide NbC in superalloy V3 after the solution at 1473 K (1200 °C) at each soaking time is greater than that after the solution at 1443 K (1170 °C). The optimal solution temperature and soaking time for 15Cr-22Ni iron-base superalloys V1 and V2 were determined to be 1443 K (1170 °C) for 2 hours and 1443 K (1170 °C) for 1 h, respectively. There are still large NbC and Fe<sub>2</sub>Nb-type Laves phase particles in superalloy V3 irrespective of the solution temperature of 1443 K (1170 °C) and 1473 K (1200 °C). The solution temperature of 1503 K (1230 °C) was not employed for superalloy V3 because this temperature is higher than the solidus temperature of the superalloy V3 [1487 K (1214 °C), calculated with Thermo-Calc software (TCFE8 database)].

The results in this article show that the area fractions of eutectic carbides NbC and Laves phase in the 15Cr-22Ni iron-base superalloys before the solution increase with increasing the niobium content up to 1.00 mass pct, and the area fraction of Laves phase significantly increases with increasing the niobium content from 1.00 mass pct to 1.40 mass pct. The amount of eutectic carbides NbC in the superalloy V1 and V2 is much larger than that of Fe<sub>2</sub>Nb-type Laves phase, whereas an opposite trend is present for superalloy V3. Zhou *et al.*<sup>[26]</sup> demonstrated that the mass ratio of Nb to C in alumina-forming austenitic stainless steel exerts a significant effect on the types of Nb-containing precipitates. In the current 15Cr-22Ni iron-base superalloy, the main type of the precipitates is NbC if the mass ratio of Nb/C is < 40, and Fe<sub>2</sub>Nb-type Laves phase becomes

the dominant type of precipitate when the Nb/C mass ratio is > 40. The formation of large Fe<sub>2</sub>Nb-type Laves phase would consume the strengthening elements of Nb and Mo, which reduce the solution strengthening effect of these alloying elements. The large Laves phase in the 15Cr-22Ni iron-base superalloy should be dissolved during solution.

### E. Vickers Hardness of 15Cr-22Ni Iron-Base Superalloy

Figure 19 shows the Vickers hardness of 15Cr-22Ni iron-base superalloy at different solution temperatures and soaking times. Note that the Vickers hardness of the superalloy decreases gradually with the extension of the soaking time. The hardness of both superalloys V1 and V3 almost linearly decreases significantly over time at different solution temperatures. The hardness of superalloy V2 also decreases (but not significantly) over time at the solution temperatures of 1473 K (1200 °C) and 1503 K (1230 °C). The decrease in the Vickers hardness is mainly caused by the coarsening of the grains in view of the stability of the austenite matrix during solution treatment.

Second-phase particles generally experience Ostwald ripening effect and coarsen at high temperatures, and thereafter these second-phase particles will no longer provide a strengthening effect on the superalloy.<sup>[13]</sup> The grain growth is dependent on the migration of the grain boundary and solute atom diffusion. Palmiere<sup>[22]</sup> reported that carbon and nitrogen in steel cannot be fully consumed to form Nb(CN) precipitates. The individual influence of grain size, solution strengthening and dislocation strengthening on the hardness cannot be separated. Considering the influence of dislocation strengthening and the block of grain boundary on dislocation slip, Hall and Petch<sup>[44,45]</sup> developed a model (*i.e.*, Eq. [25]) to describe the relationship between the hardness and the grain size.

$$H = H_0 + k_{HP}d_{average}^{-1/2} \quad [25]$$

where  $H$  and  $H_0$  are the hardnesses of the alloy at different times,  $k_{HP}$  is the Hall-Petch coefficient, and  $d_{average}$  is the average grain size.

The role of niobium in the Vickers hardness of 15Cr-22Ni iron-base superalloy is achieved mainly through acting on the grain sizes (which can be learned from Eq. [25]) and providing solution strengthening. Figures 3 and 19 show that the relationship between Vickers hardness and grain size strictly follows the Hall-Petch formula (*i.e.*, Eq. [25]). The Vickers hardness of superalloys V1 and V3 decreases almost linearly over soaking time at different solution temperatures because of increased grain size. However, the decrease in the hardness of superalloy V2 at the solution temperatures of 1443 K (1170 °C) and 1473 K (1200 °C) with the extension of soaking time is not significant because of the compensation for the weakening of fine grain strengthening (the increase in the grain size over time, see Section III-A-a) with the solution strengthening contributed by the soluble niobium atoms.

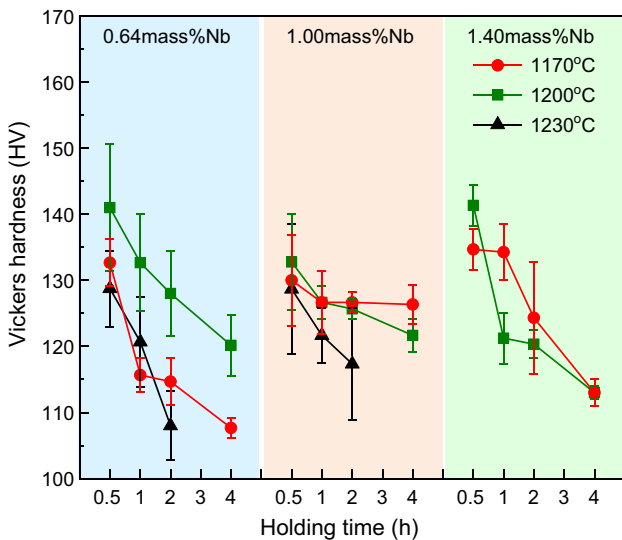


Fig. 19—Vickers hardness of 15Cr-22Ni iron-base superalloy after the solution at different holding temperatures and soaking time.



#### IV. CONCLUSIONS

The effects of solution temperatures and soaking time on the microstructure, precipitates and Vickers hardness of a newly developed 15Cr-22Ni iron-base superalloy with different niobium contents were studied. The main conclusions are summarized as follows:

(1) The austenite grains of 15Cr-22Ni iron-base superalloy with different niobium contents obviously grow up with the increase in the soaking time and solution temperature. The solution temperature is the dominant factor in determining austenite grain growth. The grain coarsening temperature is 1473 K (1200 °C) irrespective of the niobium content of the superalloy and soaking time.

(2) Increasing the niobium content of the superalloy increases the amount of Fe<sub>2</sub>Nb-type Laves phase in as-forged superalloy and the dissolution temperature of Fe<sub>2</sub>Nb-type Laves phase as well as significantly enhances the competition of the dissolution between Laves phase and eutectic carbides NbC. The precipitates in the as-forged superalloy with 0.64 and 1.00 mass pct of niobium are eutectic carbides NbC (main precipitates in the amount), besides Fe<sub>2</sub>Nb-type Laves phase. Increasing the niobium content up to 1.40 mass pct, Fe<sub>2</sub>Nb-type Laves phase became the main precipitates in the as-forged superalloy, and a large amount of eutectic carbides NbC was also observed.

(3) Fe<sub>2</sub>Nb-type Laves phase in the superalloy with 0.64 and 1.00 mass pct of niobium fully dissolves at each solution temperature and soaking time. The amount of eutectic carbides NbC decreases with the increase in the solution temperature irrespective of the soaking time. For the solution of the superalloy with 1.40 mass pct Nb at 1443 K (1170 °C), the amount of Fe<sub>2</sub>Nb-type Laves phase and NbC almost linearly decreases over time, and the Laves phase fully dissolves at 1473 K (1200 °C) and soaking time of 0.5 h. The amount of eutectic carbides NbC in the superalloy containing 1.40 mass pct Nb is larger after the solution at 1473 K (1200 °C) compared with that at 1443 K (1170 °C). This is because the complete dissolution of Laves phase at 1473 K (1200 °C) contributes the presence of a larger amount of soluble niobium in matrix, bringing a higher concentration product of soluble Nb and C.

(4) Increasing the niobium content of the superalloy increases the amount of nano-sized NbC particles, which enhances the pinning effect on the grain boundaries and inhibits austenite grain growth during solution. Nano-sized NbC particles coarsen and dissolve at the solution temperature of 1473 K (1200 °C), and consequently the pinning force on the grain boundary migration becomes weak, resulting in the abnormal growth of part of large grains.

(5) A model for describing and predicting grain growth is developed. The developed model successfully describes and predicts the austenite grain growth of 15Cr-22Ni iron-base superalloy with different niobium contents under different solution conditions.

(6) The Vickers hardness of the superalloy containing 0.64 and 1.40 mass pct Nb decreases with increasing solution temperature and soaking time. The Vickers hardness of the superalloy with 1.00 mass pct Nb did not decrease obviously with the increase in the soaking time at the solution temperatures of 1443 K (1170 °C) and 1473 K (1200 °C).

#### ACKNOWLEDGMENTS

The financial support by the National Natural Science Foundation of China (Grant Nos. 51874026 and 52074027) and the Fundamental Research Funds for the Central Universities (Grant No. FRF-AT-20-13) is greatly acknowledged. The authors are also grateful to the financial support from the State Key Laboratory of Advanced Metallurgy (Grant No. 41621024).

#### CONFLICT OF INTEREST

On behalf of all authors, the corresponding author states that there is no conflict of interest.

#### REFERENCES

1. M. Seifollahi, S.H. Razavi, Sh. Kheirandish, and S.M. Abbasi: *Phys. Met. Metall.*, 2020, vol. 121, pp. 284–90.
2. B.S. Rho, S.W. Nam, and X. Xie: *J. Mater. Sci.*, 2002, vol. 37, pp. 203–09.
3. P.D. Tiedra, Ó. Martín, and M. San-Juan: *J. Alloys Compd.*, 2016, vol. 673, pp. 231–36.
4. K. Kobayashi, K. Yamaguchi, M. Hayakawa, and M. Kimura: *Int. J. Fatigue*, 2008, vol. 30, pp. 1978–84.
5. Y. Ning, S. Huang, M.W. Fu, and J. Dong: *Mater. Charact.*, 2015, vol. 109, pp. 36–42.
6. M. Zhao, Z. Guo, H. Liang, and L. Rong: *Mater. Sci. Eng. A.*, 2010, vol. 527, pp. 5844–51.
7. Y. Toda, Y. Nakamura, N. Harada, A. Kaseya, N. Kobata, Y. Yamabe-Mitarai, and O. Umezawa: *Mater. Sci. Eng. A*, 2020, vol. 797, pp. 140104.
8. Z. Sun, P.D. Edmondson, and Y. Yamamoto: *Acta Mater.*, 2018, vol. 144, pp. 716–27.
9. S. Sui, Z. Li, C. Zhong, Q. Zhang, A. Gasser, J. Chen, Y. Chew, and G. Bi: *Compos. Part B.*, 2021, vol. 215, p. 108819.
10. S. Chen, C. Zhang, Z. Xia, H. Ishikawa, and Z. Yang: *Mater. Sci. Eng. A.*, 2014, vol. 616, pp. 183–88.
11. Q. Yu and Y. Sun: *Mater. Sci. Eng. A.*, 2006, vol. 420, pp. 34–38.
12. Y. Zhang, X. Li, Y. Liu, C. Liu, J. Dong, L. Yu, and H. Li: *Mater. Charact.*, 2020, vol. 169, p. 110612.
13. E. Pu, W. Zheng, Z. Song, K. Zhang, F. Yang, H. Lu, and H. Dong: *Mater. Sci. Eng. A.*, 2017, vol. 705, pp. 335–47.
14. B. Piekarski: *Mater. Charact.*, 2001, vol. 47, pp. 181–6.
15. H. Lu, H. G. W. Liang, J. Li, G. Zhang, and T. Li: *Mater. Des.*, 2020, vol. 188, pp. 108477.
16. Y. Zhang, H. Wang, H. Sun, and G. Chen: *Mater. Sci. Eng. A.*, 2020, vol. 798, p. 140236.
17. C. Dong, Z. Liu, Z. Chen, H. Bao, X. Wang, and Z. Liu: *J. Alloys Compd.*, 2020, vol. 825, p. 154106.
18. Y. Xu, J. Liu, Y. Zhao, and Y. Jiao: *Philos. Mag.*, 2021, vol. 101, pp. 77–95.
19. M. Shirdel, H. Mirzadeh, and M.H. Parsa: *Mater. Charact.*, 2014, vol. 97, pp. 11–17.

20. A. Chamanfar, S.M. Chentouf, M. Jahazi, and L.P. Lapierrre-Boire: *J. Mater. Res. Technol.*, 2020, vol. 9, pp. 12102–14.
21. M. Maalekian, R. Radis, M. Militzer, A. Moreau, and W.J. Poole: *Acta Mater.*, 2012, vol. 60, pp. 1015–26.
22. E.J. Palmiere, C.I. Garcia, and A.J. Ardo: *Metall. Mater. Trans. A.*, 1994, vol. 25, pp. 277–86.
23. P.R. Rios: *Acta Mater.*, 1997, vol. 45, pp. 1785–89.
24. P.R. Rios and M.E. Glicksman: *Acta Mater.*, 2006, vol. 54, pp. 5313–21.
25. V.Y. Novikov: *Mater. Lett.*, 2012, vol. 68, pp. 413–15.
26. D. Zhou, W. Zhao, H. Mao, Y. Hu, X. Xu, X. Sun, and Z. Lu: *Mater. Sci. Eng. A.*, 2015, vol. 622, pp. 91–100.
27. C. Wagner: *Thermodynamics of Alloys*, Addison-Wesley Press, Cambridge, 1952, p. 51.
28. R.C. Sharma, V.K. Lakshmanan, and J.S. Kirkaldy: *Metall. Trans. A.*, 1984, vol. 15, pp. 545–53.
29. G. Solis-Bravo, M. Merwin, and C.I. Garcia: *Metals.*, 2020, vol. 10, p. 89.
30. L.M. Fu, H.R. Wang, W. Wang, and A.D. Shan: *Mater. Sci. Technol.*, 2011, vol. 27, pp. 996–1001.
31. H.R. Wang and W. Wang: *Mater. Sci. Technol.*, 2008, vol. 24, pp. 228–32.
32. I.M. Lifshitz and V.V. Slyozov: *J. Phys. Chem. Solids.*, 1961, vol. 19, pp. 35–50.
33. Q.L. Yong: *Second Phases in Structural Steel*, Metallurgical Industry Press, Beijing, 2006.
34. G.S. Rohrer: *Metall. Mater. Trans. B.*, 2010, vol. 41, pp. 457–94.
35. B.R. Patterson and Y. Liu: *Metall. Trans. A.*, 1992, vol. 23, pp. 2481–82.
36. T. Gladman and D. Dulieu: *Met. Sci.*, 1974, vol. 8, pp. 167–76.
37. F.J. Humphreys and M. Hatherly: *Recrystallization and Related Annealing Phenomena*, Elsevier, New York, 2012.
38. P.A. Beck, J.C. Kremer, and L. Demer: *Phys. Rev.*, 1947, vol. 71, p. 555.
39. E. Anelli: *ISIJ Int.*, 1992, vol. 32, pp. 440–49.
40. N. Raghunathan and T. Sheppard: *Mater. Sci. Technol.*, 1989, vol. 5, pp. 542–47.
41. K.A. Annan, C.W. Siyasiya, and W.E. Stumpf: *ISIJ Int.*, 2018, vol. 58, pp. 333–39.
42. W.J. Liu: *Metall. Mater. Trans. A.*, 1995, vol. 26, pp. 1641–57.
43. S. Uhm, J. Moon, C. Lee, J. Yoon, and B. Lee: *ISIJ Int.*, 2004, vol. 44, pp. 1230–37.
44. E.O. Hall: *Proc. Phys. Soc. Sect. B London.*, 1951, vol. 64, pp. 747–53.
45. N.J. Petch: *J. Iron Steel Inst.*, 1953, vol. 174, pp. 25–28.

**Publisher's Note** Springer Nature remains neutral with regard to jurisdictional claims in published maps and institutional affiliations.